

Interplay between spin-glass-like and non-Fermi-liquid behavior in $\text{CeNi}_{1-x}\text{Rh}_x\text{Sn}$

A. Ślebarski,^{1,2} M. B. Maple,² R. E. Baumbach,² and T. A. Sayles²

¹*Institute of Physics, University of Silesia, 40-007 Katowice, Poland*

²*Department of Physics and Institute for Pure and Applied Physical Sciences,*

University of California, San Diego, La Jolla, California 92093, USA

(Received 26 February 2008; revised manuscript received 30 May 2008; published 26 June 2008)

The effect of doping in CeNiSn has been studied by measurements of electrical resistivity, magnetic susceptibility, and specific heat for polycrystalline samples of $\text{CeNi}_{1-x}\text{Rh}_x\text{Sn}$. It was observed that the semimetallic compound CeNiSn transforms into a Kondo semiconductor upon the substitution of 2% of Rh for Ni. We show that the narrow Kondo-insulator gap formation can be associated with disorder-induced f -electron localization. The magnetic properties of the system gradually evolve from magnetic glassy state, observed for $0 < x < 0.08$, to non-Fermi-liquid (NFL) behavior, when the Rh doping increases. The series of $\text{CeNi}_{1-x}\text{Rh}_x\text{Sn}$ exhibits NFL behavior in the vicinity of a zero-temperature magnetic phase transition, which is associated with spin-glass-like ordering due to chemical substitution. The detailed investigations of magnetic properties with decreasing Rh concentration suggest an interplay between the spin-glass-like (glassy state) and NFL ground states for the concentration region $x < 0.08$. On the basis of the experimental results, we propose a schematic phase diagram on the T - x plane and demonstrate the rationale for the existence of a quantum critical point at $x_c \approx 0.08$.

DOI: [10.1103/PhysRevB.77.245133](https://doi.org/10.1103/PhysRevB.77.245133)

PACS number(s): 71.27.+a, 72.15.Qm

I. INTRODUCTION

Kondo insulators (KI) are characterized as a class of non-magnetic narrow-gap Δ semiconductors and semimetals, which exhibits a metallic heavy-fermion (HF) state at $T > \Delta$. CeRhSb is an example of a full-gap semiconductor with Δ of about 8 K,¹ whereas CeNiSn is known as a semimetallic system.^{2,3} For CeNiSn , evidence for a small energy gap/pseudogap at the Fermi energy (ϵ_F) is inferred from tunneling spectroscopy,^{4,5} electrical resistivity,⁶ specific heat,⁷ NMR,³ and inelastic neutron scattering studies.⁸ Recently, it was reported⁹ that the formation of the KI gap is due to the presence of a collective spin-singlet Kondo state, which is singled out by the magnetic susceptibility $\chi(T) \rightarrow 0$ with decreasing T , and activated behavior of the resistivity $\rho(T)$. As a consequence, the universal scaling law $\rho(T)\chi(T) = \text{const}$ represents a universal characteristic of these strongly correlated electron systems and completes the definition of a Kondo semiconductor at $T \rightarrow 0$ from an experimental point of view. The small gap/pseudogap insulator CeNiSn does not fit, however, into this class of KI. Very pure samples of CeNiSn exhibit quasimetallic conductivity,⁶ rather than semiconducting behavior, and magnetic susceptibility, which increases when $T \rightarrow 0$ (Ref. 10), whereas a small amount of impurities open a gap in the density of states (DOS).¹¹

A systematic study has shown that the gap in doped CeNiSn is very sensitive to the degree of hybridization V between the f electron and conduction electron (c) states. This is a simple consequence of the dependence of the f - c exchange interaction on either the number of carriers (composition) or pressure, since the f - c exchange interaction results in a competition between the intrasite Kondo and the intersite Ruderman-Kittel-Kasuya-Yoshida (RKKY) interaction.¹² The KI discussed within the periodic Anderson model provides an insulating state for a \mathbf{k} -independent intrasite hybridization and for an even number of electrons per atom,¹³ as is

the case for CeRhSb . When the number of carriers is changed, the gap is expected to disappear even for $T=0$. In the context of this picture, a previous alloying study showed that the substitution of Sn for Sb drives the system $\text{CeRhSb}_{1-x}\text{Sn}_x$ from Kondo semiconducting state into a non-Fermi-liquid (NFL) HF metallic state above the critical concentration $x_c \approx 0.12$.⁹ It was also shown that this quantum critical behavior is associated with the localization of correlated f electrons at very low temperatures.

In the system $\text{CeNi}_{1-x}\text{Rh}_x\text{Sn}$, the carrier concentration diminishes upon Rh substitution for Ni. Therefore, we expect to find similar behavior to that reported for the series $\text{CeRhSb}_{1-x}\text{Sn}_x$. In this paper we present a schematic phase diagram for $\text{CeNi}_{1-x}\text{Rh}_x\text{Sn}$ on the T - x plane, based on electrical resistivity and magnetic susceptibility data. We find that the narrow pseudogap in CeNiSn is associated with the collective Kondo spin-singlet state formation, singled out directly by the reduced magnetic susceptibility $\chi(T)$ when $T \rightarrow 0$ and by the universal scaling law $\rho(T)\chi(T) = \text{const}$. The gap is strongly reduced with Rh substitution. We also report the spin-glass-like (SG) behavior (e.g., magnetic glassy state) for $0 < x \leq 0.06$ resulting from the localized Ce magnetic moments and an interplay between SG and NFL behavior.

II. EXPERIMENTAL DETAILS

Pure CeNiSn and CeRhSn samples were first prepared by arc melting weighed amounts of each component. Both samples were carefully examined by x-ray-diffraction analysis and found to be single phase with the orthorhombic ϵ - TiNiSi structure (space group $Pnma$) and hexagonal structure of the Fe_2P type (space group $P\bar{6}2m$), respectively. The dilute $\text{CeNi}_{1-x}\text{Rh}_x\text{Sn}$ alloys were then prepared by diluting nominal compositions of the master compounds. To ensure homogeneity, each sample was turned over and remelted sev-

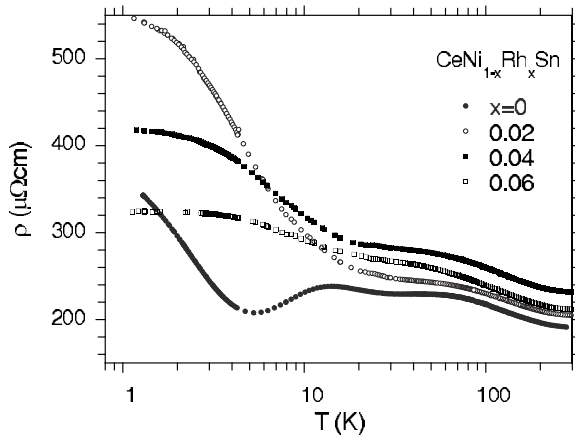


FIG. 1. Temperature dependence of the resistivity ρ for $\text{CeNi}_{1-x}\text{Rh}_x\text{Sn}$ system for $x \leq 0.06$ in the Kondo insulating regime.

eral times and then annealed at 800 °C for 2 weeks. The samples were carefully examined by x-ray-diffraction analysis and found to be single phase of the ϵ -TiNiSn-type structure for the $x < 0.4$, and of the Fe_2P -type structure for $x \geq 0.7$. The sample composition, determined using x-ray energy-dispersive spectroscopy, was found to be very close to the nominal value, consistent with negligible losses (less than 0.2% of the mass) produced during the melting procedure. dc magnetization and ac magnetic susceptibility measurements were performed for different dc fields and frequencies in the temperature range $2 \leq T \leq 300$ K, using quantum design superconducting quantum interference device (SQUID) magnetometers. The zero-field-cooled (ZFC) susceptibility was measured by heating in a magnetic field after zero-field cooling to 1.9 K; the field-cooled (FC) susceptibility was measured by applying a measuring field at high temperatures and then cooling in the field. A standard four-terminal ac technique was used to measure the electrical resistance of each sample, from which the electrical resistivity was calculated by multiplication with the geometrical factor. The absolute resistivity value was obtained within $\pm 3\%$ due to the uncertainty in the geometrical factor. However, the relative resistivity change can be measured with much better accuracy of about 10^{-4} .

III. RESULTS

A. Resistivity

In Fig. 1, we display the temperature dependence of the electrical resistivity ρ for the samples $x \leq 0.06$. In Figs. 2 and 3, we show the $\Delta\rho$ data obtained for the compositions $0.08 \leq x \leq 0.4$ and $x \geq 0.7$, respectively, where $\Delta\rho = \rho(\text{CeNi}_{1-x}\text{Rh}_x\text{Sn}) - \rho(\text{LaNiSn})$ is shown in Fig. 2, and $\Delta\rho = \rho(\text{CeNi}_{1-x}\text{Rh}_x\text{Sn}) - \rho(\text{LaRhSn})$ is shown in Fig. 3. The curves in Fig. 1 exhibit an activated behavior, where $\rho \sim \exp(\Delta/T)$ describes the low-temperature regime with an activation energy $\Delta = \Delta(x)$ as listed in Table I. The maxima in $\rho(T)$ at ~ 20 K and ~ 70 K were interpreted as being due to an anisotropic and incoherent Kondo scattering effect in the presence of a crystalline electric field.²

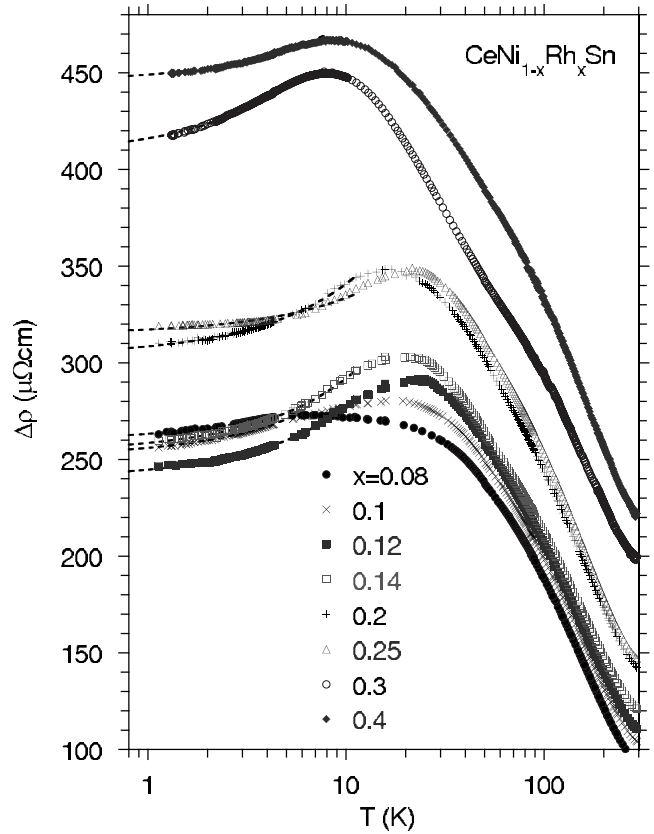


FIG. 2. $\text{CeNi}_{1-x}\text{Rh}_x\text{Sn}$; temperature dependence of the resistivity $\Delta\rho = \rho(\text{CeNi}_{1-x}\text{Rh}_x\text{Sn}) - \rho(\text{LaNiSn})$ for the Rh concentration $0.08 \leq x \leq 0.4$. The dotted lines are the fits of $\rho(T) = A + BT^n$ to the data at the temperature range $T < \sim 10$ K. The $n \approx 1$ value is obtained from the best fits for all ρ curves.

For the metallic regime ($x > 0.06$), the resistivity displays a maximum, which appears in the range of $T_{\text{max}} \sim 10\text{--}70$ K, depending on the concentration x . Above T_{max} ,

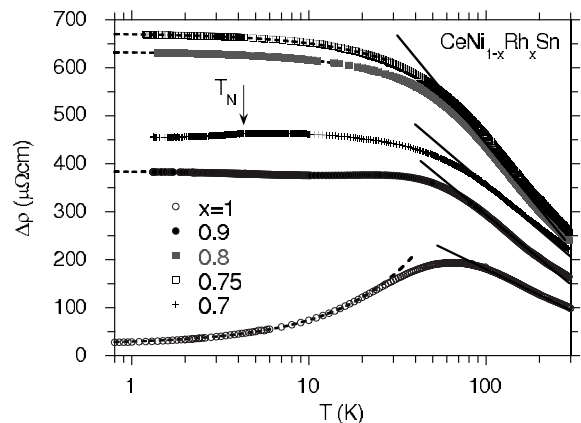


FIG. 3. The resistivity $\Delta\rho(T) = \rho(\text{CeNi}_{1-x}\text{Rh}_x\text{Sn}) - \rho(\text{LaRhSn})$ vs $\ln T$ for $\text{CeNi}_{1-x}\text{Rh}_x\text{Sn}$, where $0.7 \leq x \leq 1$. For CeRhSn the electrical resistivity $\Delta\rho$ is well fitted by the expression $\Delta\rho(T) = A + BT^n$; $n = 0.93$ (dotted line) below $T = 23$ K, while for the samples $x = 0.9, 0.8,$ and 0.75 $\Delta\rho$ was found to follow the form of equation $\Delta\rho = A - BT^n$ with $n \approx 1$ for $T < \sim 25$ K (dotted lines). The line marks the $\rho \sim -\ln T$ dependence.

TABLE I. ZFC susceptibility and the resistivity parametrization of the CeNi_{1-x}Rh_xSn samples; conductivity gap Δ is obtained from the best fit of activated expression $\rho(T)=\rho_0 \exp(\Delta/T)$ to experimental data. The activated behavior is obtained in the temperature range 2–5 K for CeNiSn and between ~ 5 and ~ 20 K for the remaining CeNi_{1-x}Rh_xSn samples. The electrical resistivity $\Delta\rho$ is well fitted by the expression $\Delta\rho=A \pm BT^n$; $n \approx 1$ with $B > 0$ for CeRhSn and $B < 0$ for samples $x=0.9, 0.8,$ and 0.75 in the temperature range $T < 10$ K for $0.08 \leq x \leq 0.4,$ or $T < 25$ K for $x > 0.7$.

x	structure	$\chi = \chi_0 + C/(T - \theta); C = 0.807$		$\chi \sim T^{-n}$		$\rho = \rho_0 \exp(\Delta/T)$	$\Delta\rho = A \pm BT^n$			
		χ_0 (10^4 emu/mol)	θ (K)	n	ΔT (K)	Δ (K)	A ($\mu\Omega$ cm)	B ($\mu\Omega$ cm/K ^{n})	n	
0	<i>Pnma</i>					1.22				
0.02	<i>Pnma</i>			0.21	$T_f < T < 36$	1.97				
0.04	<i>Pnma</i>			0.26	$T_f < T < 18$	1.68				
0.06	<i>Pnma</i>			0.23	$T_f < T < 19$	0.92				
0.08	<i>Pnma</i>	5.3	-72.7	0.27	$T < 18$		260.3	3.0	0.94	
0.1	<i>Pnma</i>	3.6	-125.8	0.24	$T < 13$		252.5	3.9	0.94	
0.12	<i>Pnma</i>	3.7	-110.4	0.20	$T < 13$		239.4	4.4	0.93	
0.14	<i>Pnma</i>	3.6	-102.1	0.20	$5 < T < 13$		255.1	3.8	0.99	
0.2	<i>Pnma</i>	2.2	-107.7	0.48	$T < 13$		288.3	3.8	0.95	
0.25	<i>Pnma</i>	6.0	-92.6	0.55	$T < 16$		297.2	1.1	1.0	
0.3	<i>Pnma</i>	3.2	-85.6	0.30	$6.6 < T < 26$		406.5	9.5	0.84	
0.4	<i>Pnma</i>	1.5	-82.6	0.70	$T < 14$		445.2	3.8	0.85	
0.7	<i>P$\bar{6}2m$</i>	9.6	-17.8							
		$T_N = 4.25$ K, $C = 0.48$								
0.75	<i>P$\bar{6}2m$</i>	11.5	-11.3	0.62	$T < 14$		672.1	-2.4	1.05	
		$C = 0.22$								
0.8	<i>P$\bar{6}2m$</i>			0.27	$T < 3.5$		633.8	-2.0	0.96	
0.9	<i>P$\bar{6}2m$</i>			0.54	$T < 6$		684.6	-1.4	0.96	
1	<i>P$\bar{6}2m$</i>			0.50	$T < 5$		23.86	5.9	0.93	
		$T > \sim 60$ K						$T < \sim 10$ K		

a well-defined logarithmic dependence with negative slope is observed, while below T_{\max} , $\rho \sim T^\epsilon$, where $\epsilon \approx 1$, indicating non-Landau-Fermi-liquid behavior (see, Figs. 2 and 3). The x -dependent maximum and the $\Delta\rho \sim -\ln T$ behavior give evidence that the resistivity maximum results from a competition between quantum coherence (i.e., itineracy of $4f$ electrons due to the hybridization of the f -electron states with the conduction electron states) and the thermal disorder acting as a decoherence factor (the $4f$ -electron states are localizing for $T > T_{\max}$). Note that above T_{\max} , the magnetic susceptibility approaches a Curie-Weiss (CW) law for $4f^1$ localized moments on Ce, as discussed below.

As shown in Fig. 3 for $0.7 < x < 1$, $\Delta\rho(T)$ exhibits behavior characteristic of a Kondo-impurity system with a Kondo temperature of about 50 K. Namely, $\Delta\rho \sim -\ln T$ over a wide temperature range, and $\Delta\rho \sim 1 \pm aT^n$ at $T < T_K/2$, with $n \approx 1$ and $a > 0$ for CeRhSn or $a < 0$ for $0.7 < x < 1$. The $\Delta\rho(T)$ dependences for $0.7 < x < 1$ are quite different than that obtained for CeRhSn. A possible reason for the difference is atomic disorder, which can lead to the negative temperature coefficient of the resistivity,¹⁴ as observed for many strongly disordered metals.

B. Magnetic susceptibility

In Fig. 4, we present the dc magnetic susceptibility curves ($\chi = M/H$) measured for orthorhombic CeNi_{1-x}Rh_xSn samples ($x \leq 0.4$) in the ZFC regime. The inset displays the susceptibility measured for the samples $0.02 \leq x \leq 0.08$ in ZFC and FC regimes in a dc field of 100 Oe; the $\chi(T)$ data display hysteretic features typically related to the development of a SG state below a freezing temperature T_f for $0 < x \leq 0.06$.

In Fig. 5, we present the results of ac susceptibility measurements. Figure 5(a) displays the maximum of the real component χ' of $x=0.02$ for a frequency of 500 Hz and an applied ac field of 3 Oe. The χ'' component does not show any anomaly at T_f . A similar χ' behavior was observed for the samples $x=0.04$ and 0.06 . As the rhodium concentration approaches the value $x=0.08$, the freezing temperature goes to zero, whereas the peak displayed by $\chi(T)$ and the irreversibility between the ZFC and FC branches is quite reduced, as shown in Fig. 5(a). Panel (b) displays the frequency-dependent maxima of χ'' for the sample $x=0.02$ in the alternating field with an amplitude of 3.9 Oe, which is the other typical signature of SG behavior. On the other hand the imaginary components χ'' show a very weak anomaly at T_f

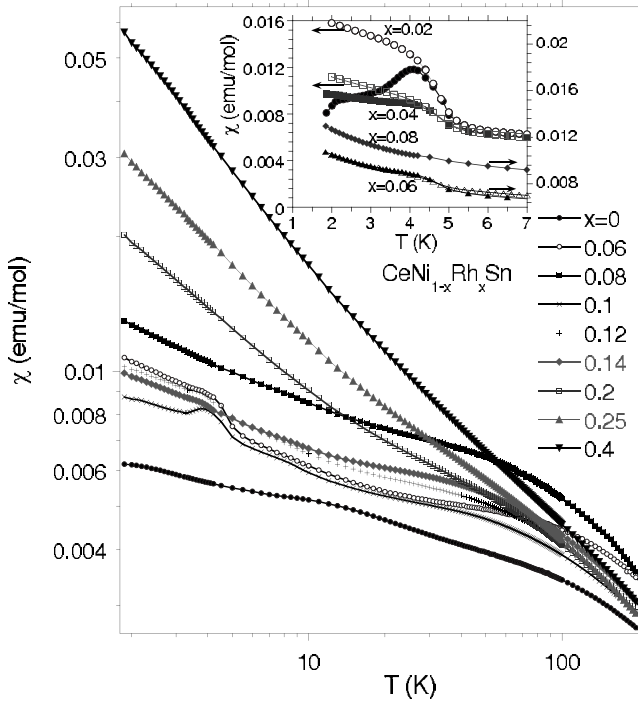


FIG. 4. Temperature dependence of the ZFC dc susceptibility ($H=100$ Oe) in log-log scale for $\text{CeNi}_{1-x}\text{Rh}_x\text{Sn}$ system when $x \leq 0.4$. In the low-temperature range $\chi(T) \sim T^{-n}$ with exponent $n \approx 0.2$ for the samples $x < 0.2$, and $n \approx 0.5$ for $x \geq 0.2$ (details in Table I). The inset displays ZFC and FC dc susceptibility measured in the magnetic field $H=100$ Oe, where irreversibility is observed for $x \leq 0.06$.

for low frequencies ($\nu < 100$ Hz). A very similar χ'' behavior was reported for the $\text{Y}_{1-x}\text{U}_x\text{Pd}$ system with magnetically inhomogeneous state in which there is interplay between a spin-glass phase and the NFL behavior, induced by disorder.¹⁵ In Fig. 5(b), however, the dynamic behavior is different than that reported in Ref. 15. Namely, the amplitude of χ' decreases, and the shift of χ' maximum is downwards in temperature with decreasing frequency in the frequency range $\nu \leq 100$ Hz, but the amplitude and position of the χ' maximum is practically constant in the frequencies $\nu \geq 500$ Hz. The low-frequency susceptibility curves of $x = 0.02$ (also of $x = 0.06$) look more like those of a short-range antiferromagnet with a small frequency dependence of χ' and almost no χ'' . Such a short-range antiferromagnet may display a glassy behavior associated with atomic disorder, which can lead to magnetic inhomogeneity.¹⁶

All of the SG features disappear for rhodium concentrations larger than 0.08 in the concentration range $0.08 \leq x < 0.4$, and χ' follows a modified CW law. χ' of CeNiSn shows a rapid increase with decreasing T below 3 K consistent with the presence of paramagnetic impurities with concentration less than 1%. Finally, in Fig. 6, we present magnetization M versus H data for $\text{CeNi}_{0.98}\text{Rh}_{0.02}\text{Sn}$, which show a hysteresis loop below temperature T_f . The similar M versus H behavior was also observed for the compounds with $x = 0.04$ and 0.06 , whereas for concentrations of Rh greater than $x = 0.06$, the magnetization shows no hysteresis at the lowest temperatures. All of these measurements strongly

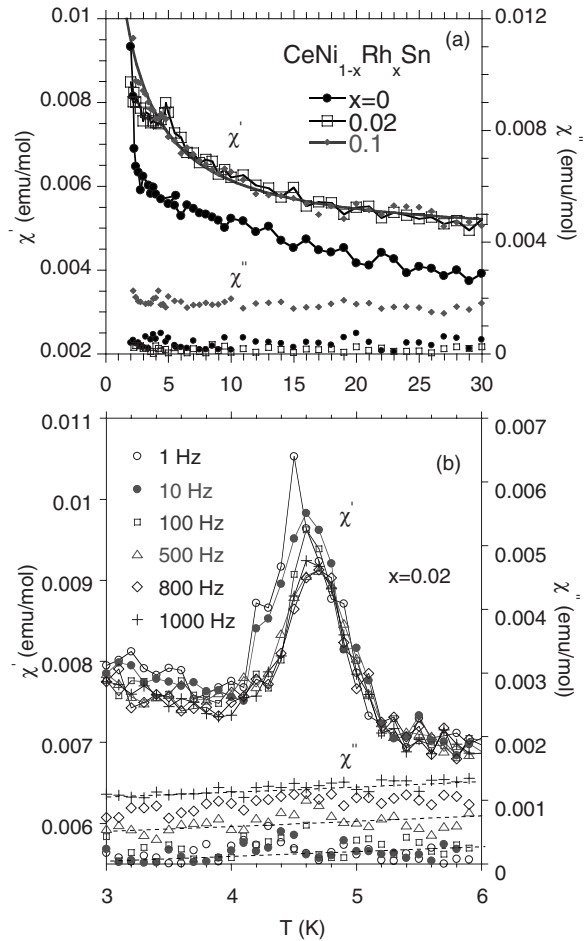


FIG. 5. Real χ' and imaginary χ'' components of ac magnetic susceptibility. In panel (a); the $\chi(T)$ ac data ($\nu=500$ Hz, $H=3$ Oe) shows characteristic SG peak for $x=0.02$, whereas the remaining samples are paramagnetic. The solid line fits the modified CW equation to the χ' data for the sample $x=0.1$; the fitting parameters are: $\chi_0=0.0045$ emu/mol, $\gamma=0.02$, and $\theta=-2.2$ K. Panel (b) shows the ac susceptibility measured at different frequencies with an applied field of 3.9 Oe.

support the interpretation that there exists a SG state in the compounds of the $\text{CeNi}_{1-x}\text{Rh}_x\text{Sn}$ system containing less than 6% of Rh. However, the SG phenomena presented in Figs. 4 and 5 are not quite typical for an intrinsic spin-glass transition, namely the magnetic susceptibility is sensitive to the magnitude of the applied field, and the peak of χ' is not evidently shifted toward lower temperatures as the frequency is larger than 100 Hz and decreases. Likewise, the observed freezing temperature does not change very much with the Rh concentration, which is in contrast with the fact that the irreversibility between the ZFC and FC branches tends to zero. These behaviors would mean that the SG (glassy state) transition is not an intrinsic effect and is probably due to the local atomic disorder (will be discussed latter).

One should note that the susceptibilities displayed in Fig. 4 also have a weak feature for samples $0.06 < x \leq 0.12$, which is not of SG-like origin. The χ_{ac} data do not reveal the glassy phase for this x -concentration range. Likewise, the magnetization does not show any hysteresis loops. In Fig. 7,

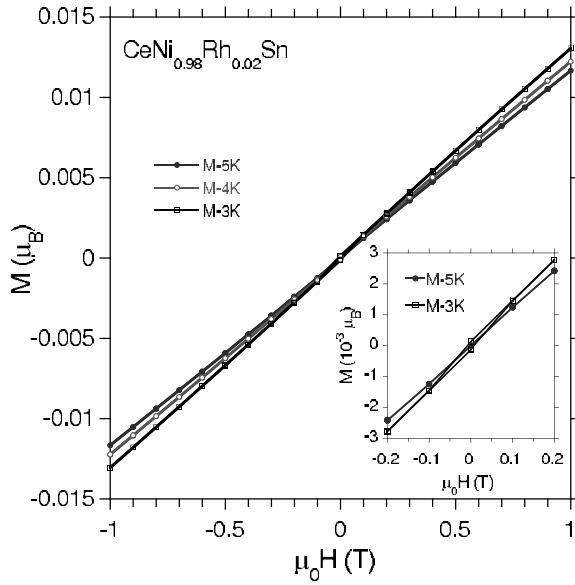


FIG. 6. The magnetization M vs magnetic field for $\text{CeNi}_{0.98}\text{Rh}_{0.02}\text{Sn}$.

we present the ZFC and FC susceptibility for $\text{CeNi}_{0.9}\text{Rh}_{0.1}\text{Sn}$ measured at $H=100$ Oe and 1 kOe. In the temperature range $T > 100$ K, χ follows a modified CW law (see Table I) with an effective magnetic moment typical for Ce^{3+} atoms ($2.54 \mu_B$). The inset shows that this maximum is strongly reduced in a magnetic field. Similar field and frequency dependences were found for the other samples $x=0.12$ and 0.14 , which also display the maximum. The nature of this maximum could be explained by the formation of antiferromagnetic correlations. It will be discussed on the basis of the periodic Anderson model.¹³

Finally, in Fig. 8, we summarize the susceptibility data for $\text{CeNi}_{1-x}\text{Rh}_x\text{Sn}$ for $x \geq 0.7$. At temperatures higher than 150 K, the behavior for samples with $x > 0.8$ is characteristic of valence or spin fluctuations, as is often seen for Ce compounds. CeRhSn has a weak and broad χ maximum at about 175 K, while χ for $\text{CeNi}_{0.1}\text{Rh}_{0.9}\text{Sn}$ and $\text{CeNi}_{0.2}\text{Rh}_{0.8}\text{Sn}$ in-

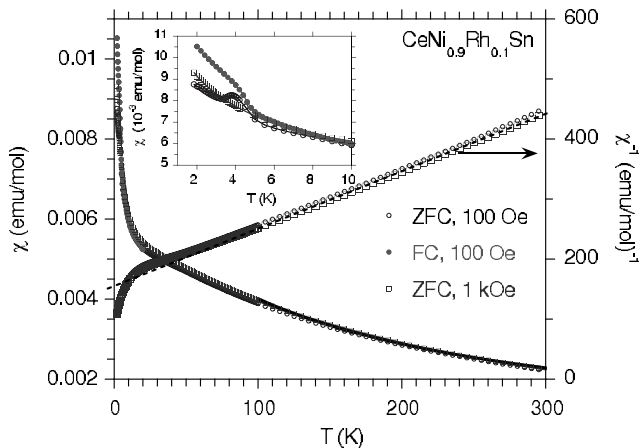


FIG. 7. ZFC and FC Susceptibility for $\text{CeNi}_{0.9}\text{Rh}_{0.1}\text{Sn}$ at different magnetic fields. The dotted line is a modified Curie-Weiss fit to the data (details in the inset).

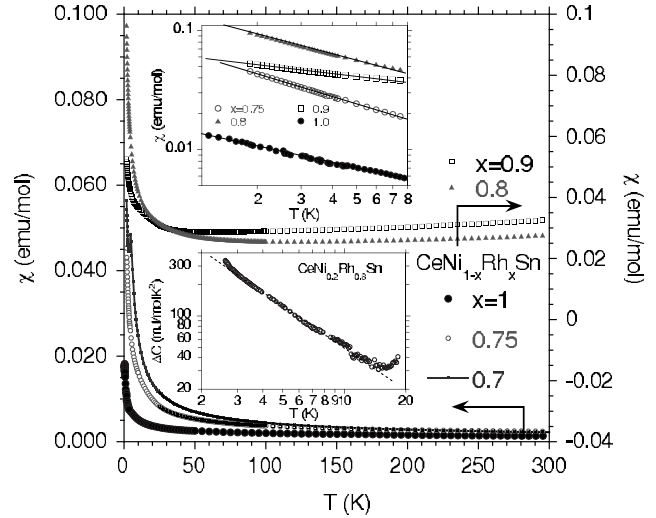


FIG. 8. $\text{CeNi}_{1-x}\text{Rh}_x\text{Sn}$; temperature dependence of the ZFC susceptibility for $x \geq 0.7$. The ac magnetic susceptibility χ' measured in an applied field of 10 Oe and at different frequencies ($\nu=50, 100, 500$, and 1000 Hz) also shows weak maximum at $T_N=4.25$ K for the sample $x=0.7$, however, without any frequency dependence. The first inset shows the $\chi(T)$ data in the log-log scale with $\chi(T) \sim T^{-n}$ behavior ($n \approx 0.5$, Table I). The second inset shows the $\Delta C = C(\text{CeNi}_{1-x}\text{Rh}_x\text{Sn}) - C(\text{LaRhSn})$ data plotted as $\Delta C/T$ vs T in the log-log scale. $\Delta C(T)/T \sim T^{-n}$, where $n=3/2$.

creases with increasing T , suggesting a maximum at higher temperatures. In contrast, for $x=0.7$ and $x=0.75$, the susceptibility follows a modified CW law (Table I) over a wide temperature range. The negative paramagnetic temperatures $\theta = -11.3$ for the 70% Rh sample suggest the localization of the f -electron states and AF ordering near the critical concentration $0.7 < x_c < 0.8$ on the Rh-rich side of the series. One should note that the divergent character of χ shown in the inset of Fig. 8 for $x > 0.7$ can be attributed to quantum critical behavior $\chi \sim T^{-n}$ ($n \approx 0.5$) in the whole metallic (NFL) regime $0.7 < x \leq 1$.

C. Specific heat

Evidence that strong electronic correlations are present in the $\text{CeNi}_{1-x}\text{Rh}_x\text{Sn}$ system is provided by the large magnitude of the electronic specific-heat coefficient $\gamma_0 \equiv C(T \rightarrow 0)/T$, which reaches a value of ~ 190 mJ/mol K^2 for $\text{CeNi}_{0.98}\text{Rh}_{0.02}\text{Sn}$, ~ 120 mJ/mol K^2 for $\text{CeNi}_{0.92}\text{Rh}_{0.08}\text{Sn}$, and 150 mJ/mol K^2 for $\text{CeNi}_{0.2}\text{Rh}_{0.8}\text{Sn}$, as seen in plots of $C(T)/T$ vs T^2 (not shown). In Fig. 9, we plot the specific-heat $\Delta C/T$ data versus T on a log-log scale, where $\Delta C = C(\text{CeNi}_{1-x}\text{Rh}_x\text{Sn}) - C(\text{LaNiSn})$. By subtracting the heat capacity of pure LaNiSn , we observed for $x=0.02$ a power-law increase of $\Delta C/T$ in the temperature range 6–13 K, i.e., above the spin-glass-paramagnetic phase transition. The singular part of the specific heat in this T region is parametrized by the power law $\Delta C/T = cT^{-n}$ (dotted lines in the figure) with exponent $n \approx 0.25$, similar to that obtained from the susceptibility $\chi \sim T^{-n}$ scaling, while below 6 K $\Delta C/T$ deviates from the power-law behavior and exhibits a pronounced maxima at 6 K and 3 K, respectively. The first feature is

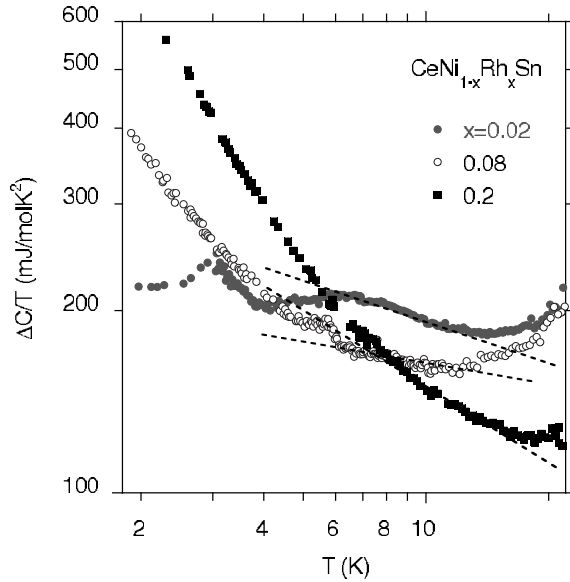


FIG. 9. $\text{CeNi}_{1-x}\text{Rh}_x\text{Sn}$; specific heat $\Delta C/T$ vs T for samples $x = 0.02$, 0.08 , and 0.2 in the log-log scale; $\Delta C = C(\text{sample}) - C(\text{LaNiSn})$. For $6 < T < 13$ K, $\Delta C(T)/T \sim T^{-n}$ with $n=0.25$ for the sample with $x=0.02$, $n=0.20$ for the sample with $x=0.08$, and $n=0.52$ for sample with $x=0.2$. At the lowest temperatures ($T < 6$ K), $\Delta C/T$ displays different T^{-n} behavior for samples $x = 0.08$ and 0.2 with n values of about 0.8 and 1.0 , respectively.

linked with pseudogap formation on the HF Fermi surface in $\text{CeNi}_{0.98}\text{Rh}_{0.02}\text{Sn}$, moreover, $\Delta C/T$ shows a linear variation $\Delta C/T = a + bT$ in $\Delta T \approx 2$ K regime below the maximum at $T \sim 6$ K, which is a direct evidence for the opening of the narrow pseudogap in the Kondo system.³ With increasing Rh concentration x from 0.02 to 0.08 , this maximum at 6 K disappears in the temperature dependence of $\Delta C/T$, suggesting for the samples $x > 0.06$ the recovery of the DOS at the Fermi level. The systematic evolution of the Kondo-insulator/semimetal gap as a function of x is well known for $\text{CeNi}_{1-x}\text{M}_x\text{Sn}$, when Ni is substituted by the other metal M , e.g., by Pt (Ref. 17) or Co (Ref. 18). Usually, the doping larger than 8% – 10% quite removes the semiconducting gap in CeNiSn . We therefore did not provide the detailed specific-heat investigations for the samples $0 < x \leq 0.06$ in order to claim the evolution of the pseudogap with increasing Rh concentration in $\text{CeNi}_{1-x}\text{Rh}_x\text{Sn}$.

Measurements of the specific heat on $\text{CeNi}_{0.98}\text{Rh}_{0.02}\text{Sn}$ (see Fig. 9) clearly reveal a phase transition at ~ 3 K, which presumably corresponds to the SG ordering, also seen in the magnetic susceptibility data. In Fig. 9, the SG ordering was not found for the remaining samples $x=0.08$ and 0.2 . For the samples with $x=0.08$ and $x=0.2$, $\Delta C/T$ varies as T^{-n} for $T < 6$ K, where $n=0.8$ and 1.0 , respectively, while in the range 6 – 13 K, there is a different power-law behavior with exponent $n=0.20$ for $x=0.08$ and $n=0.52$ for $x=0.2$. The values of the power-law exponent n obtained from the $C(T)/T$ data above T_f and independently from the $\chi(T)$ data are in reasonable agreement within experimental resolution, suggesting that the NFL behavior can be described by the Griffiths model.¹⁹ This model predicts power-law behavior of $C(T)/T$ and $\chi(T)$ with similar power-law exponents. How-

ever, the low-temperature ($T < 6$ K) dependence $\Delta C/T \sim T^{-n}$ (where n is almost two times larger) can be related to another effect, which results from disorder. It is likely that a statistical distribution of Ni and Rh atoms over the same crystallographic sites can locally change the coupling between Ce atoms, due to the different local charge distributions, which is strongly dependent on the atomic disorder. This can lead to possible magnetic instabilities, such as glassy state or AF correlations. We note that the low- T n exponent is larger when the Rh doping increases (Fig. 9), which suggests the disorder effect.

IV. DISCUSSION

A. Properties in the regime: $x \leq 0.4$

From the evolution of the x dependences of the susceptibility χ and resistivity ρ , the following main conclusions emerge. First, the electrical conductivity exhibits activated behavior for Rh concentrations smaller than 8% . The substitution of Rh for Ni in $\text{CeNi}_{1-x}\text{Rh}_x\text{Sn}$ decreases the number of carriers by one per formula unit. Nevertheless, this produces an enhanced activated resistivity with a gap size $\Delta \approx 2$ K for $\text{CeNi}_{0.98}\text{Rh}_{0.02}\text{Sn}$, i.e., almost twice that obtained for the semimetallic CeNiSn . This means that the Rh impurities stabilize the semiconducting gap. Such a stabilization of the Kondo insulating state upon substitution leads to the localization of $4f$ electrons, as is evidenced by the formation of the localized spin-glass state as shown in Figs. 4 and 5. Further increase of the Rh concentration x decreases the width of the gap (Table I), which is quite reduced for concentration $x=0.08$. The gap, if associated with the collective-Kondo spin-singlet state formation, should be singled out by an intrinsic magnetic susceptibility $\chi(T)$ reduction when $T \rightarrow 0$, which was discussed recently.⁹ This is, however, not the case for CeNiSn and Rh-doped samples because of the impurities which locate the conduction bands in the Kondo gap. In Fig. 10(a), CeNiSn exhibits a sharp upturn in the susceptibility at low temperatures. This upturn is well described by the presence of Ce interstitial impurities with a concentration near $y \approx 0.006$. This Ce-impurity concentration also causes the resistivity to deviate from the $\rho(T) = \rho_0 \exp(\Delta/T)$ behavior at $T < 2$ K [see Fig. 10(b)]. In Fig. 10(a), we show the raw $\chi(T)$ data (full circles) and those with the Curie term ($\chi_0 + yC/T$) subtracted from them (open circles). In effect, if considering the impurity effect either in $\chi(T)$ or $\rho(T)$ data, the scaling χ versus ρ^{-1} is clearly observed for the semimetallic CeNiSn Kondo system [see Fig. 10(c)].

Second, for $x < 0.08$ the collective bound Kondo-lattice insulating state is formed at $T < T_m$. For CeNiSn , we observed a maximum in $\chi(T)$ at $T_m \approx 11$ K [Fig. 10(a)], which determines the effective binding energy of $4f$ spins into a collective singlet (the maximum is reduced when the collective low-temperature singlet state is destroyed by thermal motion, as discussed in detail in Ref. 9 for the KI CeRhSb). For Rh-doped CeNiSn samples, the disorder creates localized states in the pseudogap region and leads to magnetic glassy state, which however, removes activated behavior when $x > 0.06$.

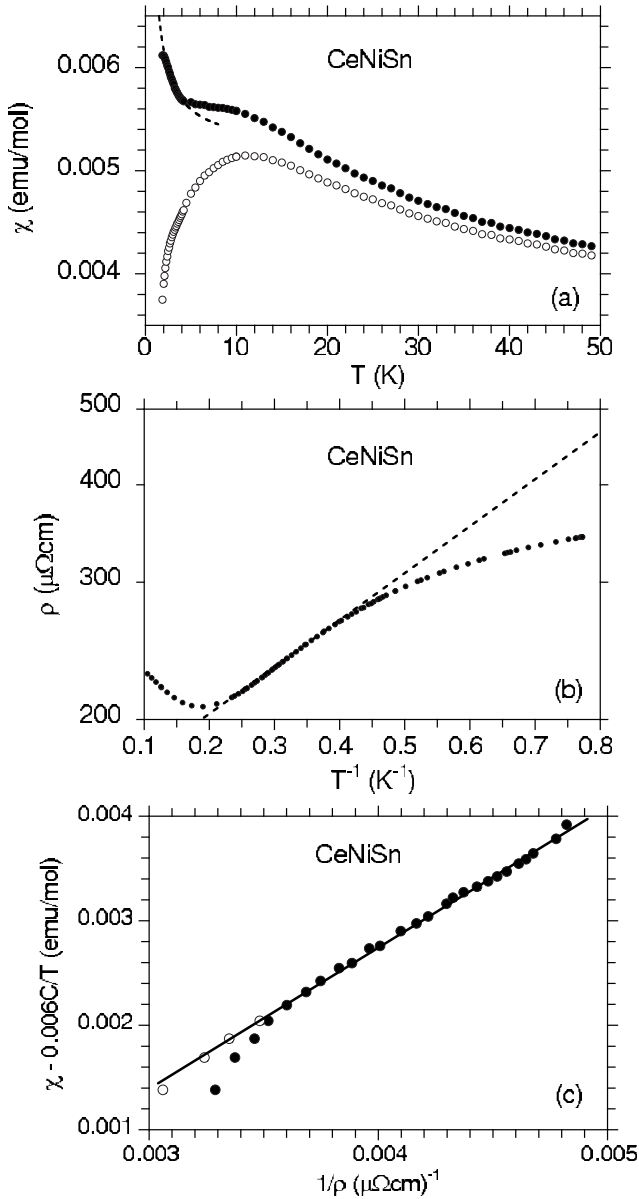


FIG. 10. ZFC magnetic susceptibility (a), and resistivity (b) for CeNiSn. In panel (b) the impurity contribution yC/T is subtracted from the raw data (open points), the dotted line is a Curie-Weiss fit to the $\chi(T)$ data due to impurities. In panel (c): linear scaling law between resistivity ρ and susceptibility $\chi - yC/T$, $y=0.006$. The open points represent resistivity corrected by the impurity effect.

Third, as the rhodium concentration approaches the value $x=0.08$, the freezing temperature tends to zero and all of the spin-glass features disappear, at which point a NFL ground state emerges as the Rh doping increases (see Table I). Figure 4 illustrates the scaling $\chi \sim T^{-n}$ on a double logarithmic scale. As shown in Table I the n value is about 0.2 for $0 < x < 0.2$, whereas for the samples $x \geq 0.2$, the exponent $n \approx 0.5$. The divergence of χ at $x=0.08$ means that CeNiSn, when doped, approaches a magnetic phase-transition point at $T=0$. What we observe in our system is the formation of magnetic states, in which there is an interplay between a glassy phase when $x < 0.08$ or AF correlations for $0.08 < x < 0.12$, and a nonmagnetic phase with an NFL contribution

to the susceptibility. Therefore, we suggest that the NFL properties observed in this system are related to the progressive disorder-induced weakening of the glassy state observed for $x < 0.08$, giving rise to a Griffiths phase as x approaches the quantum critical point (QCP) at $x=0.08$. Since the divergence near the weak AF behavior is observed for the systems with $x=0.1-0.14$, it is suggested that there are singular NFL phases in this x region, i.e., with a line of singularities at $T=0$ along the x axis. However, this suggestion has to be checked at much lower temperatures.

The paramagnetic Curie temperature θ extrapolated from the temperature region $T > 60-100$ K is negative and of the order of 100 K (Table I), suggesting an interplay of the magnetic interactions between Ce moments and the Kondo effect. The standard simple impurity Kondo model predicts $T_K \approx |\theta|/4$ (Ref. 20), which yields a reasonable estimate for the Kondo temperature $T_K \approx 25$ K. These values of T_K roughly correlate with the values of T_{coh} at which the $\Delta\rho(T)$ curves show a maximum in Fig. 2. For CeNi $_{1-x}$ Rh $_x$ Sn with $0.06 < x < 0.4$, one observes a resistivity maximum at $T_{\text{max}} \sim 20$ K and a $\rho \sim -\ln T$ dependence at higher temperatures. This behavior is characteristic of Kondo lattices with a coherence effect below T_{max} . The standard expression for the virtual bound-state width²¹ predicts that $k_B T_{\text{max}} \sim \pi V^2 N(\epsilon_F)$, where V is the magnitude of intra-atomic hybridization of the f states with the conduction electrons and $N(\epsilon_F)$ is the DOS in the bare conduction band at the Fermi energy. Assuming $N(\epsilon_F) \sim 0.1(\text{eV atom})^{-1}$ and $V \sim 0.1$ eV (see Ref. 22), one obtains $T_{\text{max}} \sim 35$ K, which agrees reasonably well with the experimental findings. Theoretically, the quantum coherence (i.e., the appearance of heavy quasiparticle states) is associated with the effective Kondo (hybridization) temperature T_K , not with the temperature T_{max} , which represents a good characteristic quantity from an experimental point of view. The low lying excitations in the Anderson- (Kondo-) lattice state appear below $T_K < T_{\text{max}}$. If the effective f -electron bandwidth is of the order $T_K \sim 2(V^2/|\epsilon_f|)(1-n_f)$, where $\epsilon_f < 1$ eV is the location of the f level in the valence band and $n_f \approx 0.95$ (Ref. 23), then the estimated value of $T_K \sim 20$ K is in good agreement with our susceptibility and resistivity data. The low value of T_K suggests the nonmagnetic character of the correlated quantum liquid, which can form either a heavy fermi liquid or NFL state, depending on the strength of the exchange magnetic interactions (RKKY) in relation to the Kondo interactions. The phase diagram of this system is shown in Fig. 11.

B. Properties in the metallic regime: $x > 0.7$

Recently, we classified CeRhSn as a NFL system.²³ Its low-temperature behavior was modeled in terms of the Griffiths phase.¹⁹ In this model, the combined effect of sufficiently strong disorder and the competition between the Kondo and the RKKY interactions can lead to a pocket of magnetically ordered regions (Griffiths phase), where the order-parameter dynamics may determine thermodynamic properties of the system in the vicinity of a QCP and are due to the tunneling between different configurations. We have shown that $\Delta\rho \sim T^\epsilon$, with $\epsilon \approx 1$ (see Fig. 3), while the specific

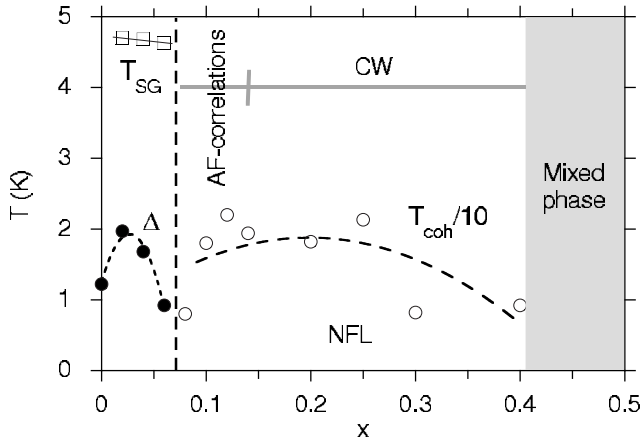


FIG. 11. Schematic phase diagram for $\text{CeNi}_{1-x}\text{Rh}_x\text{Sn}$ systems. Temperature Δ is obtained from the fit of expression $\rho(T) = \rho_0 \exp(\Delta/T)$ to the resistivity data in the Kondo insulating regime. T_{SG} is a temperature of the maximum in the χ ac data, T_{coh} is considered as T_{max} in the $\Delta\rho(T)$.

heat, $C(T)/T$, and $\chi(T)$ vary as T^{-n} , with $n \approx 0.5$. We also reported²⁴ that the specific heat data for CeRhSn obey the relationship $C(T)/T = \gamma + \delta T^2 \ln(T/T_{sf})$ for $6 < T < 25$ K, representing the Rh d spin-fluctuation contribution $T^3 \ln(T/T_{sf})$ to the specific heat (T_{sf} is the spin-fluctuation temperature and γ is the linear coefficient enhanced by the mass enhancement factor m^*/m_0). Our recent Fermi surface analysis performed from the *ab initio* calculations for the similar compound CeRhSn₂ showed that there are some parallel sections of the sheets, which might generate *nesting* instabilities and be responsible for the spin-fluctuation effect.²⁵ In Fig. 3 the coherence temperature $T_{\text{max}} \approx 60$ K, i.e., about three times larger than that of the components $x < 0.4$. This behavior is well understood, because of the larger value of $V^2N(\epsilon_F)$ obtained for CeRhSn. In Fig. 8 the susceptibility of the samples with $x=0.8$ and 0.9 shows a tendency to form a maximum above room temperature, which signals the effect of spin fluctuations similar to those observed for CeRhSn. Likewise, the specific heat data obey the expression $C(T)/T = \gamma + \delta T^2 \ln(T/T_{sf})$ for the sample $\text{CeNi}_{0.2}\text{Rh}_{0.8}\text{Sn}$ with the fitting parameters: $\gamma = 106.7$ mJ/mol K², $\delta = 0.44$ mJ/mol K⁴, and $T_{sf} = 6.1$ K, representing a spin-fluctuation contribution $T^3 \ln(T/T_{sf})$ in the range $6 < T < 20$ K. The reference level ρ_0 increases with decreasing x in the x range $1-0.7$ due to the atomic disorder. As a result, the samples with $x < 1$ do not display the coherence behavior in the resistivity data; however, susceptibility $\chi(T) \sim T^{-n}$ and $\Delta C(T)/T \sim T^{-n}$ (in Fig. 8) indicate NFL-like behavior for this concentration region.

C. CeNiSn; further comments

The stability of the paramagnetic vs magnetic ground state in the Kondo-lattice limit¹³ is strongly dependent on the

onsite hybridization magnitude V and the number of electrons n_e . Doradziński and Spalek¹³ (DS) discussed the possible magnetic phases in the periodic Anderson model and obtained the phase diagram on the $V-n_e$ plane, which provides a qualitative account of experimental results on the series of Ce-ternary intermetallics.²⁴ In the DS diagram, CeNiSn is located on the line $n_e \approx 2$ in the KI region, very close to critical value of $V \approx 0.3$ eV, which separates the KI and antiferromagnetic Kondo-insulator (AKI) phases. Our recent XPS measurements reported that the hybridization energy V for CeRhSn is a few times smaller than that obtained for CeNiSn (Ref. 24). We also noted that V decreases with doping impurities into the KI CeNiSn and CeRhSb. Therefore, the doping effect can easily vary the KI state to AKI state. On the base of this theoretical model one can explain the short-range ordering or SG state in the KI limit, when the number of electrons n_e is almost two.

V. CONCLUDING REMARKS

The compound $\text{CeNi}_{1-x}\text{Rh}_x\text{Sn}$ exhibit unconventional power-law dependences in their physical properties, which are linked to the influence of quantum phase transitions in their $T-x$ phase diagram. Experimental study of magnetic properties confirms the evolution of a magnetic glassy state at the Kondo-insulator region $0 < x < 0.08$ into NFL behavior, which is induced by disorder. Our magnetic and specific-heat measurements for the $\text{CeNi}_{1-x}\text{Rh}_x\text{Sn}$ system with $x < 0.4$ can be adequately interpreted in terms of a disorder-induced Griffiths phase model. The transition from Kondo-insulator region to a metallic region is discussed as a function of variable valence-electron number induced by substitution of Rh for Ni and of the accompanying effect of the change of hybridization energy V . CeNiSn is discussed as a semimetal with a pseudogap at the Fermi level. It was found that the impurities open this Kondo-insulator gap in CeNiSn. When the impurity effect is considered, then the scaling $\chi\rho = \text{const}$, characteristic of the Kondo insulator state, was obtained for CeNiSn.

ACKNOWLEDGMENTS

One of us (A.Ś.) is grateful for the hospitality at University of California, San Diego (UCSD), and would like to express his appreciation to the Kosciuszko Foundation for support during his visit. He also thanks the Polish Ministry of Science and Higher Education for financial support from Project No. 1 P03B 052 28. The authors are also very grateful to Josef Spalek for discussion. Research at UCSD was supported by the U. S. Department of Energy under Grant No. DE-FG02-04ER46105.

- ¹S. K. Malik and D. T. Adroja, *Phys. Rev. B* **43**, 6277 (1991).
- ²T. Takabatake, F. Teshima, H. Fujii, S. Nishigori, T. Suzuki, T. Fujita, Y. Yamaguchi, J. Sakurai, and D. Jaccard, *Phys. Rev. B* **41**, 9607 (1990).
- ³K. Nakamura, Y. Kitaoka, K. Asayama, T. Takabatake, G. Nakamoto, H. Tanaka, and H. Fujii, *Phys. Rev. B* **53**, 6385 (1996).
- ⁴T. Ekino, T. Takabatake, H. Tanaka, and H. Fujii, *Phys. Rev. Lett.* **75**, 4262 (1995).
- ⁵T. Ekino, T. Takabatake, H. Tanaka, and H. Fujii, *Physica B* **206-207**, 837 (1995).
- ⁶T. Takabatake, Y. Echizen, T. Yoshino, K. Kobayashi, G. Nakamoto, H. Fujii, and M. Sera, *Phys. Rev. B* **59**, 13878 (1999).
- ⁷A. Brückl, K. Neumaier, D. Einzel, K. Andres, S. Flaschin, G. M. Kalvius, G. Nakamoto, and T. Takabatake, *J. Low Temp. Phys.* **115**, 291 (1999).
- ⁸H. Kadowaki, T. Sato, and H. Yoshizawa, *J. Phys. Soc. Jpn.* **63**, 2074 (1994).
- ⁹A. Ślebarski and J. Spałek, *Phys. Rev. Lett.* **95**, 046402 (2005); J. Spałek, A. Ślebarski, J. Goraus, L. Spałek, K. Tomala, A. Zarzycki, and A. Hackemer, *Phys. Rev. B* **72**, 155112 (2005).
- ¹⁰T. Takabatake, G. Nakamoto, T. Yoshino, H. Fujii, K. Izawa, S. Nishigori, H. Goshima, T. Suzuki, T. Fujita, K. Maezawa, T. Hiraoka, Y. Okayama, I. Oguro, A. A. Menovsky, K. Neumaier, A. Brückl, and K. Andres, *Physica B* **223-224**, 413 (1996).
- ¹¹J. Spałek and A. Ślebarski, *Acta Phys. Pol. A* **114**, 7 (2008).
- ¹²S. Doniach, *Physica B & C* **91**, 231 (1977).
- ¹³J. Spałek and R. Doradziński, in *Magnetism and Electronic Correlations in Local-Moment Systems: Rare Earth Elements and Compounds*, edited by M. Donath, P. A. Dowben, and W. Nolting (World Scientific, Singapore, 1998), p. 387; R. Doradziński and J. Spałek, *Phys. Rev. B* **58**, 3293 (1998); for brief review, see: J. Spałek and R. Doradziński, *Acta Phys. Pol. A* **96**, 677 (1999); **97**, 71 (2000).
- ¹⁴J. H. Mooij, *Phys. Status Solidi A* **17**, 521 (1973).
- ¹⁵S. D. Wilson, P. Dai, D. T. Adroja, S.-H. Lee, J.-H. Chung, J. W. Lynn, N. P. Butch, and M. B. Maple, *Phys. Rev. Lett.* **94**, 056402 (2005); M. A. López de la Torre, J. Rodríguez Fernández, K. A. McEwen, and M. B. Maple, *Phys. Rev. B* **74**, 014431 (2006); M. B. Maple, N. P. Butch, E. D. Bauer, V. S. Zapf, P.-C. Ho, S. D. Wilson, Pengcheng Dai, D. T. Adroja, S.-H. Lee, J.-H. Chung, and J. W. Lynn, *Physica B (Amsterdam)* **378-380**, 911 (2006).
- ¹⁶M. Tokumoto, Y. Nishihara, K. Oka, and H. Unoki, *Nature (London)* **330**, 48 (1987).
- ¹⁷S. Nishigori, H. Goshima, T. Suzuki, T. Fujita, G. Nakamoto, T. Takabatake, H. Fujita, and J. Sakurai, *Physica B (Amsterdam)* **186-188**, 406 (1993).
- ¹⁸T. Takabatake, G. Nakamoto, H. Tanaka, Y. Bando, H. Fujii, S. Nishigori, H. Goshima, T. Suzuki, T. Fujita, I. Oguro, T. Hiraoka, and S. K. Malik, *Physica B (Amsterdam)* **199-200**, 457 (1994).
- ¹⁹R. B. Griffiths, *Phys. Rev. Lett.* **23**, 17 (1969); A. H. Castro Neto, G. Castilla, and B. A. Jones, *ibid.* **81**, 3531 (1998).
- ²⁰A. Hewson, *The Kondo Problem to Heavy Fermions* (Cambridge University Press, Cambridge, 1993).
- ²¹P. W. Anderson, *Phys. Rev.* **124**, 41 (1961).
- ²²A. Ślebarski, *J. Alloys Compd.* **423**, 15 (2006); A. Ślebarski and J. Spałek, *J. Magn. Magn. Mater.* **310**, e85 (2007).
- ²³A. Ślebarski, A. Jezierski, M. B. Maple, and A. Zygmunt, *Acta Phys. Pol. B* **32**, 3331 (2001); A. Ślebarski, M. B. Maple, E. J. Freeman, C. Sirvent, M. Radłowska, A. Jezierski, E. Granado, Q. Huang, and J. W. Lynn, *Philos. Mag. B* **82**, 943 (2002).
- ²⁴A. Ślebarski, J. Spałek, M. Gamża, and A. Hackemer, *Phys. Rev. B* **73**, 205115 (2006).
- ²⁵M. Gamża, A. Ślebarski, and H. Rosner, *J. Phys.: Condens. Matter* **20**, 025201 (2008).